JOURNAL OF PROPULSION AND POWER
Vol. 17, No. 6, November–December 2001

Numerical Simulation of Supersonic Airflow with Transverse Hydrogen Injection

E. von Lavante,* D. Zeitz,† and M. Kallenberg†
University of Essen, FB12, D-45127 Essen, Germany

Unsteady, three-dimensional, supersonic flow with nonequilibrium chemistry in a square channel with transverse hydrogen injection was numerically investigated. To this end, the concepts of large-eddy simulation were applied to a model supersonic combustion chamber using a three-dimensional solver of the compressible Navier–Stokes equations with chemical reactions developed by the present authors. The time-accurate computation was accelerated by an implicit method and implemented on a massively parallel computer. The results of the present three-dimensional simulation were analyzed with respect to their timewise behavior and compared, where applicable, with two-dimensional predictions and experimental data obtained by other investigators.

Nomenclature

A, B, C	=	Jacobian matrices
e	=	total energy
$\hat{\boldsymbol{F}}, \hat{\boldsymbol{G}}, \hat{\boldsymbol{H}}$	=	flux vectors
I	=	identity matrix
J	=	Jacobian of the transformation
k	=	turbulent kinetic energy
L	=	limiter
M	=	Mach number
p	=	pressure
Q	=	vector of state variables
Re	=	Reynolds number
S	=	source term
T	=	temperature
t	=	time
$\boldsymbol{U}$	=	velocity vector
u, v, w	=	velocity components
y^+	=	wall distance
Δ^+	=	forward difference
Δ^-	=	backward difference
ϵ	=	dissipation of turbulent kinetic energy
κ	=	factor in MUSCL
ξ, η, ζ	=	body-fitted coordinates
ρ	=	density

Subscripts

i	=	index in x direction
n_s	=	number of species
R	=	right
v	=	viscous
x	=	axial coordinate
0	=	total quantity

Superscripts

n	=	timestep
$\hat{}$	=	transformed values
$\bar{}$	=	time averaged

Presented as Paper 99-4902 at the 9th International Space Planes and Hypersonic Systems and Technologies Conference, Norfolk, VA, 1–5 November 1999; received 1 July 2000; revision received 15 August 2001; accepted for publication 20 August 2001.

*Professor, Department of Mechanical Engineering (Turbomachinery). Member AIAA.

†Doctoral Research Fellow, Department of Mechanical Engineering (Turbomachinery).

I. Introduction

THE recent research and development of high-speed-flight vehicles, supersonic or hypersonic, is spurring activity in corresponding areas of scientific development. The increase of scientific activities can be attributed to the reemerging interest in the concept of the scramjet. Several nations are planning uncrewed hypersonic research vehicles with the scramjet as the most logical choice of propulsion. Typical representatives of these research vehicles are the U.S. X-43A and X-43B with the ISTAR engine, developed as NASA hypersonic propulsion demonstration vehicles, the stationary PTE and GDE hypersonic scramjet test engines, the French VRR and A3CP, the French–German Japhar project, or the German ELAC/EOS two-stage vehicle. All of these research vehicles are intended to validate design tools that could be used in future development of hypersonic propulsion technology.[1,2] Detailed study of some of the physical aspects of supersonic combustion has been carried out by, for example, Brummund and Nuding.[3] The consequence of these experimental efforts is stronger involvement in the scientific area of supersonic combustion.

The simulation methods of these types of flows have reached a certain degree of maturity, offering a choice of standard spatial and timewise discretization procedures (for example, see Cox et al.[4] or Godfroy and Tissier.[5]) However, several problems remain. One of the main difficulties is the treatment of turbulence because none of the models is adequate for these complex flow cases. The interaction between the turbulent effects and the chemistry, in particular the chemical rates of reaction, is difficult to predict numerically due to the uncertainties in describing this physical phenomenon theoretically. The ability of various turbulence models to predict the mixing phenomena in a scramjet combustor was investigated by Madabhushi et al.[6] More recently, Chen and Shuen[7] completed a survey of numerical algorithms for solving the three-dimensional Navier–Stokes equations with nonequilibrium detailed chemistry. A corresponding computer code was put to practical use by, for example, Chamberlain et al.[8]

The present authors have been attempting to simulate numerically reacting flows in supersonic combustion chambers.[9,10] For laminar flows, their predictions were satisfactory; the resulting turbulent flows, however, could not be considered adequately simulated due to the absence of turbulence–chemistry interactions. The increasing complexity of the turbulence models, from simple zero-equation algebraic to two-equation (k–ϵ) models, did not bring any significant improvement. The multivariate assumed β-probability density function (PDF) approach of accounting for the turbulence–chemistry interaction, described by Narayan,[11] resulted in a gain of accuracy in the cases discussed in their paper, at a modest increase of computational cost. However, assuming the shape of the PDF also results in several problems. Here, the structure of the PDF is given, representing a significant simplification of the real physical situation.

Using the assumed PDF in the case of supersonic flows makes it impossible to consider the influence of compressibility effects or chemical reactions on the shape of the temperature PDF. Here, it is necessary to solve a full transport equation for the PDF distribution.

Usually, the strong coupling between the fluidmechanic and thermodynamic variables found in supersonic flows requires the simultaneous solution of the PDF equations for the velocities, partial densities and thermodynamic variables. The corresponding algorithm is computationally very intensive and, in the case of supersonic flows with compression shocks (present case), prohibitively expensive due to the extremely high resolution required in the shock regions. Possible help is offered by the relatively new hybrid methods, where the velocities are obtained from a Reynolds-averaged Navier–Stokes (RANS) solver and the remaining scalar quantities are given by the PDF-transport equations. This method has been introduced by, for example, Möbius et al.[12] The problem with this approach is that turbulence effects are still subject to the usual modeling with all its known problems.

A possible solution to the described problems is to employ large-eddy simulation (LES) to resolve the low-frequency fluctuations, assuming that they contain most of the turbulent kinetic energy, while implementing a subgrid model for the unresolved effects. The subgrid model should include fine-scale mixing to account more realistically for the turbulence–chemistry interactions. A modified version of the linear eddy model for subgrid combustion was developed by Chakravarthy and Menon[13] and, more recently, by Menon.[14] This subgrid model was employed for studying the properties of turbulent premixed flames in the core region of Couette flow. Arunajatesan and Menon[15] used a simpler LES model for simulations of flow in a compact incinertor. The LES equivalent to the PDF approach in the case of the RANS solver are the filtered density function (FDF) methods. These ideas are relatively recent (for example, see Colucci et al.[16]) and, therefore, are unproven on anything but the simplest test cases.

In view of the preceding discussion of the difficulty to formulate an appropriate model for the turbulence–chemistry interaction, as well as the turbulence alone, the present authors decided in the initial phase of the present project to investigate the feasibility of LES applied to a case of chemically reacting supersonic flow of the air–hydrogen system. The presence of a rather complex shock system made the use of assumed PDF distributions seem inappropriate, while a full-scale Monte Carlo approach was too computationally intensive. Lacking recent knowledge about the FDF methods, the authors decided to take a simplified approach similar to the mentioned hybrid methods. The velocities where obtained from the LES simulation in combination with a relatively simple Smagorinsky subgrid model, the scalar temperature fluctuations were obtained from the resolved values while neglecting their subgrid component, and their effect on the reaction rates was modeled. The unresolved part of the mass fractions was neglected. A justification for this assumption is given subsequently in the corresponding section of this paper.

II. Algorithm

In the present work, the flow was assumed to be compressible, viscous, and a mixture of thermally perfect species. Because of the relatively low temperature and high pressure in the present configuration, the gas mixture can be treated as in vibrational (thermodynamic) equilibrium. The governing equations were in this case the compressible Navier–Stokes equations for n_s species:

$$\frac{\partial \hat{\boldsymbol{Q}}}{\partial t} + \frac{\partial \hat{\boldsymbol{F}}}{\partial \xi} + \frac{\partial \hat{\boldsymbol{G}}}{\partial \eta} + \frac{\partial \hat{\boldsymbol{H}}}{\partial \zeta} = \frac{S}{J} \tag{1}$$

where $\hat{\boldsymbol{F}}$, $\hat{\boldsymbol{G}}$, and $\hat{\boldsymbol{H}}$ are the flux vectors in the corresponding ξ, η and ζ directions, $\boldsymbol{Q}$ is the vector of the dependent state variables $(\rho u, \rho v, \rho w, e, \rho_1, \ldots, \rho_{n_s})^T$, and J is the Jacobian of the transformation of coordinates. The details of the governing equations are given in Ref. 17.

A simple model according to Fick's law for the binary diffusion coefficient was used, along with the Sutherland equation for the viscous coefficient. The chemical reactions for the H_2–air combustion were realized with an eight-reaction and seven-specie model of Evans and Schexnayder,[18] representing a compromise between computational effort and complexity and physical reality.

Three different upwind methods were extended to chemical reaction systems and are optionally available in the present computer code. These methods are based on the work of Roe and Pike [flux-difference splitting, (FDS)],[19] van Leer (flux-vector splitting),[20] and Liou (advection-upstream-splitting method).[21] Best results were obtained with the FDS scheme, making it the exclusive choice in the present simulations.

A. Spatial Discretization

The present research mostly employed a numerical scheme based on Roe's FDS in finite volume form. This scheme was demonstrated to be accurate, with relatively low dissipation and dispersion. Depending on the type of limiter and MUSCL interpolation, this scheme was highly effective in providing accurate viscous results at a wide range of Mach numbers. In the present version, the reconstruction of the cell-centered variables to the cell-interface locations was done using a monotone interpolation as introduced by Grossmann and Cinella.[22] The interpolation slope was limited by an appropriate limiter, according to the previously published MUSCL-type procedure (for example, see Ref. 9):

$$\boldsymbol{Q}_R^n = \boldsymbol{Q}_{i+1}^{n-1} - \tfrac{1}{4} L_{i+1}\left[(1+\kappa)\Delta_{i+1}^{-} + (1-\kappa)\Delta_{i+1}^{+}\right]^{\eta-1} \tag{2}$$

using a special quadratic version of the van Albada limiter developed by the present authors:

$$L_i = \frac{2\Delta_i^{-2}\Delta_i^{+2} + \varepsilon}{\Delta_i^{-4} + \Delta_i^{+4} + \varepsilon}, \qquad \varepsilon \approx 1 \times 10^{-5} \tag{3}$$

Variation of the accuracy factor κ and switching the limiter on or off results in various schemes from simple first-order accurate up to third-order formulation. In the present work, the second-order accurate upwind biased Fromm scheme ($\kappa = 0$) and the preceding form of van Albada limiter has been used. The viscous fluxes $\boldsymbol{F}_v$, $\boldsymbol{G}_v$, and $\boldsymbol{H}_v$ were centrally differenced.

The details of this scheme, with the corresponding modifications, are given by Hilgenstock et al.[10] This includes also the positivity preserving modifications in the sense of Larrouturou and Fezoui.[23]

B. Temporal Integration

Initially, the governing equations were integrated using a semi-implicit method, with different multistage Runge–Kutta type schemes used for the explicit operator. Only the chemical source terms were treated implicitly,

$$\left\{ I - \Delta t \frac{\partial S^n}{\partial \boldsymbol{Q}^n} \right\} \frac{\partial \boldsymbol{Q}^n}{\partial t J} = \hat{S}^n - \frac{\partial \hat{\boldsymbol{F}}^n}{\partial \xi} - \frac{\partial \hat{\boldsymbol{G}}^n}{\partial \eta} - \frac{\partial \hat{\boldsymbol{H}}^n}{\partial \zeta} \tag{4}$$

The numerical effort to invert the matrix $D = I - \Delta t(\partial S^n / \partial \boldsymbol{Q}^n)$ depends on the formulation of the Jacobian of the chemical source terms. Several different forms of the Jacobian matrix, with increasing complexity and accuracy, were implemented and compared. The most obvious choice is to invert the full $n_s \times n_s$ matrix D. However, it is a problem from the numerical point of view because the inversion is CPU time consuming and the matrix D is usually ill conditioned. This approach worked, but was rather inefficient. The next possibility to simplify the matrix D consists of dropping all of the off-diagonal terms, while keeping only the diagonal terms. In our case of eight reactions with seven species, this turned out to be an effective means of accelerating the convergence, with stability limits given by the acoustic wave speeds.

However, the highly restrictive time limit, caused by the fine spatial resolution, resulted in prohibitively slow rates of convergence. Therefore, the fully implicit delta form of the governing equations

$$\left\{ I + \Delta t \frac{\partial}{\partial \xi} A + \Delta t \frac{\partial}{\partial \eta} B + \Delta t \frac{\partial}{\partial \zeta} C - \Delta t \frac{\partial S^n}{\partial \boldsymbol{Q}^n} \right\} \delta \hat{\boldsymbol{Q}}^n$$

$$= \Delta t \left(\hat{S}^n - \frac{\partial \hat{\boldsymbol{F}}^n}{\partial \xi} - \frac{\partial \hat{\boldsymbol{G}}^n}{\partial \eta} - \frac{\partial \hat{\boldsymbol{H}}^n}{\partial \zeta} \right) \tag{5}$$

was implemented. A, B, and C in Eq. (5) are the Jacobian matrices $A = \partial \boldsymbol{F}^n / \partial \boldsymbol{Q}^n$, $B = \partial \boldsymbol{G}^n / \partial \boldsymbol{Q}^n$, and $C = \partial \boldsymbol{H}^n / \partial \boldsymbol{Q}^n$. In the present work, the symmetric Gauss–Seidel relaxation procedure was chosen for the implicit operator. This scheme allows larger time steps, while formally maintaining the same time accuracy on the block boundaries as in the interior of the computational domain. Without subiterations in pseudotime, the scheme is first-order accurate in time, improving to second-order accuracy in time with the substepping.

Using a multiblock grid structure resulted in a flexible code with the possibility of working with different chemical models (nonequilibrium, equilibrium, and frozen) in different blocks. Besides, some of the blocks were selectively refined, depending on the evolving results. The present geometrical treatment of the computational domain was simple, yet flexible enough.

III. Turbulence

Previously, turbulence closure models based on statistical methods, such as the well known k–ϵ model, were used by the present authors and other investigators. The results were mixed, at best. These methods utilize or imply a certain type of averaging of the governing equations and require modeling of the correlations of all of the fluctuating quantities that represent turbulence. In the present work, the LES approach was deemed more appropriate. It separates the field variables of the turbulent flow into large-scale and small-scale quantities. The large-scale parts are computed directly by solving the filtered governing equations, whereas the unresolved small-scale quantities need to be modeled in terms of the resolved variables. This was accomplished by the subgrid-scale eddy viscosity model proposed by Smagorinsky.[24]

After the simulation was carried out for a time interval long enough (at least three periods of the lowest frequency oscillation), a timewise mean value of the state variables was computed. Assuming again that the LES resolves the major part of the turbulence spectrum, one can postulate that the resolved part of the timewise fluctuation of temperature and species concentration will be representative of the turbulence–chemistry coupling. Then, substracting, for example, the mean temperature $\tilde{T}$ from the actual time-accurate value will yield the fluctuation T'':

$$T'' = T - \tilde{T} \tag{6}$$

with similar expressions for the species concentrations. When the approach of Narayan[11] is followed, the influence of the fluctuations on the chemical reaction mechanism can be incorporated. At present, only the influence of the temperature was considered. At first, neglecting the mass-fraction fluctuations might seem unadvisable in view of the usually strong coupling of the temperature fluctuations with the partial density fluctuations. However, in the particular case simulated in the present work, where the combustion is mainly governed by the shock-induced combustion, the influence of the temperature is much more significant than that of the mass fractions. Recently, this observation has been confirmed by Sattelmayer.[25]

IV. Verification

The present numerical algorithm was subjected to verification of its temporal and spatial accuracy and consistancy. The scheme is formally second-order accurate in space because the viscous terms are obtained from second-order central differences. The scheme was first verified using the usual grid refinement study for the case of viscous flat plate flow at a freestream Mach number of $M_\infty = 0.5$. When the global error was defined as the L_2 norm of the deviation of the present solution from the Blasius solution, second-order accuracy was verified (von Lavante[26]). Next, the combination of the present solution scheme with the physical test case and a typical computational grid to be used was investigated in two dimensions using five different grids. Again, a case of transverse hydrogen injection through a two-dimensional slot of an equivalent width with the same physical parameters has been selected. Because the flow after the injection slot was highly unsteady, the length of the separated region upstream of the hydrogen injection x_{sep} represented the global parameter used for comparison. Table 1 summarizes the results. Noted that the three finest grids result in approximately the same separation length.

Table 1 Comparison of results on different grids

Internal cells	Number of blocks (Processing Units)	X_{sep}, mm
32×32	4	53
64×64	16	86
128×128	16	92
256×256	64	95
1024×1024	256	94

Table 2 Strouhal number in cylinder wake flow

Researcher	Method	Strouhal number
Lugt[27]	Experimental	0.193
Truckenbrodt[28]	Experimental	0.192
Authors	Numerical	0.194
Faden[29]	Numerical	0.198

Fig. 1 Turbulent kinetic energy, two-dimensional simulation.

The temporal accuracy was tested by simulating the two-dimensional flow about a circular cylinder with freestream Mach number $M_\infty = 0.1$ and Reynolds number $Re = 200$. The resulting Strouhal number of the vortex separation was compared with known experimental and numerical results in Table 2. The agreement was rather good.

A corresponding grid refinement study in three dimensions was, unfortunately, not feasible due to the extreme amount of computational resources necessary. When the results of the two-dimensional refinement study were considered, it was decided that a three-dimensional grid of the size 256 (x direction) $\times$ 128 (y direction) $\times$ 32 (z direction) was sufficient to resolve most of the important features in the flowfield. In particular, the two-dimensional simulations on the 128×128 grid resulted in the turbulent kinetic energy shown in Fig. 1. Although the authors fully realize the limitations of a two-dimensional simulation and would never try to call this LES, it is interesting that the location of the largest fluctuations (in the free shear layer) and the increase of turbulence intensity in the shocks could be recognized.

V. Parallel Implementation

Ideally, in a LES, turbulent eddies with as large energy contents as possible should be directly simulated, making resolutions of an order of magnitude below y^+ necessary. Because no preferential direction is assumed, this very high resolution should be applied not only normal to the solid walls, but in all spatial directions considered in that particular simulation. Additionally, the computational grid should be uniformly distributed. Clearly, even if the specified requirements are somewhat relaxed, an extremely high number of grid points (or cells in the finite volume method) have to be utilized. The corresponding computations can be carried out only on the largest computers available. A performance that is adequate for the LES is presently offered only on massively parallel computers.

Early in this work, it was decided to implement a data parallel structure because the multiblock grid system already had data exchange between the blocks built in. The parallelization was accomplished using the Message Passing Interface library using standard point-to-point communications. Only few global operations had to be used.

The production runs were carried out on a Cray T3E using 128 Processing Units. Before this machine became available, an IBM SP2 using 8 Processing Units and a cluster of Linux

personal computers using up to 12 Processing Units were also used. In the two-dimensional case, the maximum total grid size was 1024×1024 internal cells, although a 256×128 grid was mostly sufficient. The present three-dimensional simulation was executed using a $256 \times 128 \times 32$ grid, assuming symmetric flow in the crosswise direction. The more appropriate periodic boundary condition resulted in an unrestricted crosswise velocity w. Note that the Cray T3E, the IBM SP2, and, surprisingly, the Linux personal computers, based on the Pentium II CPU at 300 MHz, demonstrated approximately the same performance per Processing Unit. Furthermore, because the present application is highly computationally intensive, the times necessary for interzonal communication were relatively insignificant, resulting in very efficient parallelization of the code.

VI. Test Case Configuration

The geometry selected for the present test was relatively simple, consisting of a rectangular channel with a 0.06×0.06 m cross section. All of the opposite walls were parallel; the length of the channel was approximately 0.465 m. At a distance of 0.105 m from the leading edge of the tube, hydrogen was injected from the upper and lower wall through a dense row of small holes (0.002 m diam). The flow in these injection holes reached critical conditions. The holes were very closely spaced at a distance of 4 mm between their centers. The intention was to approximate two-dimensional flow conditions as closely as possible, thus enabling a comparison with two-dimensional simulations. Unfortunately, it will be shown later that even in this case the flow at the injection location was fully three dimensional. The basic geometry including information about the flow conditions is shown schematically in Fig. 2.

The structure of the multiblock computational grid used in the present simulation is shown in Fig. 3. The location of the H_2 injection holes, the physical size of the overall domain in meters and the various boundary conditions are also indicated. The computational grid consisted of $256 \times 128 \times 32$ internal cells, arranged in 128 blocks.

A simplified view of the flow and the shock structure close to the H_2 injection hole has been published by, among others, Ramakrishnan and Singh.[30] The dominant features of this shock system can be seen in Fig. 4.

The geometry and the boundary conditions of this configuration are described in detail by von Lavante et al.[9] At the inflow, the Mach number was $M = 2.97$, the static pressure was $p = 0.137$ MPa, and the static temperature was $T = 1300$ K. The hydrogen jet enters at sonic conditions, at a static pressure of $p = 0.4$ MPa; its static temperature was $T = 350$ K. The Reynolds number per one meter reference length was in this case $Re_x = 1.7 \times 10^7$. This case is of particular interest because has been frequently used in numerical simulations by other authors and has been experimentally investigated by, for example, Quenett.[31]

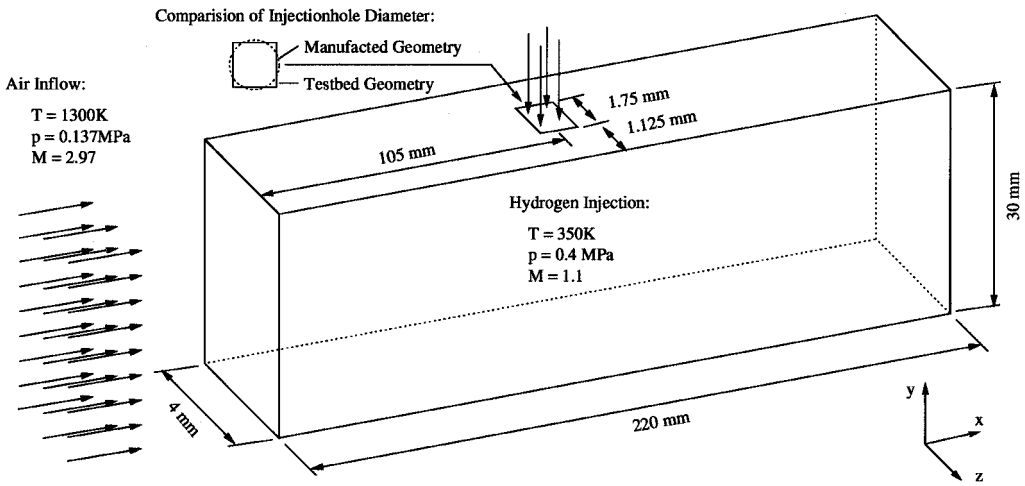

Fig. 2 Schematic of the present flow case.

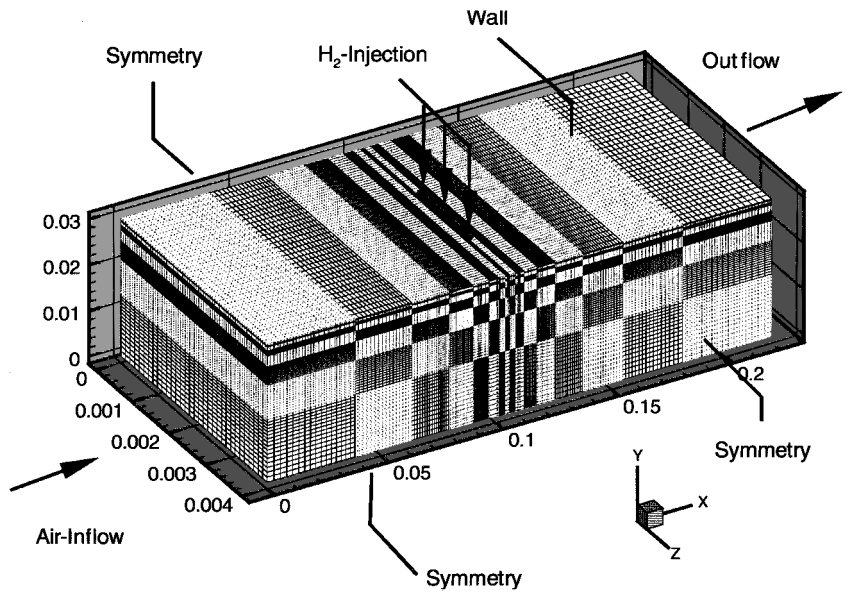

Fig. 3 View of the block-structured computational grid.

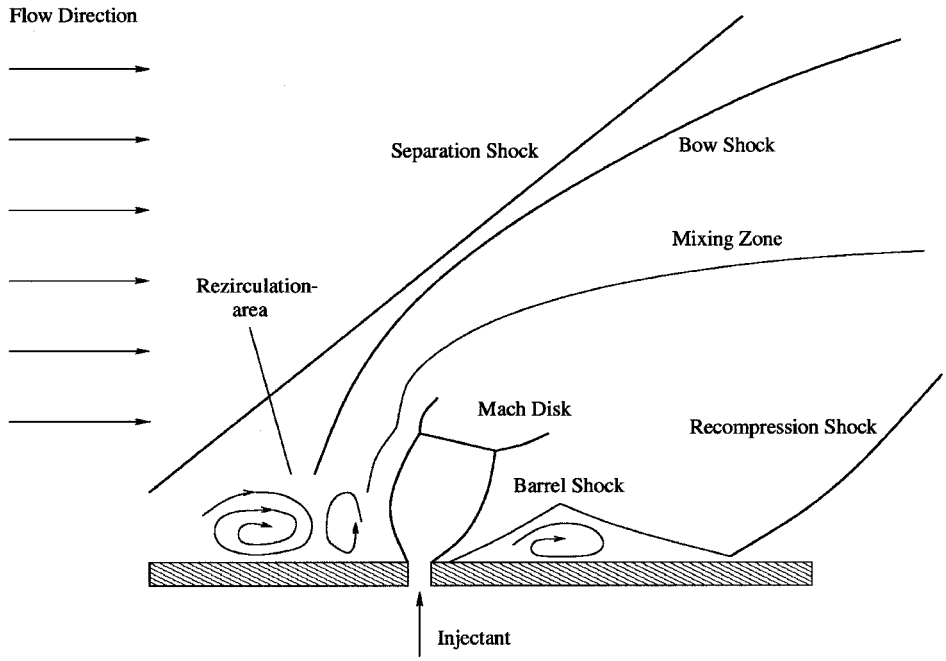

Fig. 4 Simplified view of the shock structure around the injection.

VII. Results

The three-dimensional flow simulation used the previously obtained two-dimensional data as an initial condition. The two-dimensional results were published elsewhere,[9] so that only the three-dimensional results will be discussed here. First, the timewise development of the flow as it evolves from the two-dimensional case is discussed. A comparison of the two-dimensional results with their three-dimensional equivalents demonstrates the importance of the three-dimensional effects. The three-dimensional computation was started initially from the two-dimensional flow distribution extrapolated crosswise into the third dimension. At the initial time t_0 the length of the separated region x_{sep} was 94 mm and the penetration depth of the H_2 jet, h_{pen}, was 8.9 mm. Both values agreed fairly well with the empirically determined dependency $x_{sep} = f(h_{pen})$ given by Ramakrishnan and Singh.[30] Here, f is a linear function given in graphical form. In the course of the computation, x_{sep} decreased until it reached its final average value of 29 mm at time $t_0 + 790\ \mu$s. Because of the unsteady character of the flow, the length of the separated region fluctuated about the timewise average by approximately ± 1 mm. The penetration depth reached $h_{pen} = 3.3$ mm and fluctuated by approximately 0.3 mm. Even in the three-dimensional case, the tendency of the relationship between x_{sep} and h_{pen} is preserved in that the separation length decreased with decreasing penetration depth.

In Fig. 5, instantaneous velocity vectors in the vicinity of the injection hole are shown. Clearly visible is the barrel shock, the oblique bow shock, the free shear layer behind the H_2 jet, and the separation regions upstream and downstream of the injection. The high resolution of the boundary layer can be seen in the two magnified pictures.

The flow forms a horseshoe vortex around the jet, thus relieving the pressure ahead of the injection. This flow feature, visible in Fig. 6, explains the much smaller separation region upstream of the injection hole. In Fig. 6, the complex flow at this location can be seen, including a curved bow shock, the H_2 jet, the extent of the free shear layer, and its three-dimensional shape. After leaving the injection hole at critical conditions, the jet expands and forms several Mach disks. The H_2 jet is unsteady, moving in a circular periodic motion with a frequency of approximately 8 kHz. Consequently, the flowfield downstream of it is also highly unsteady.

The same view, this time showing the water concentration, is offered in Fig. 7. Here, the separated region ahead of the H_2 jet can

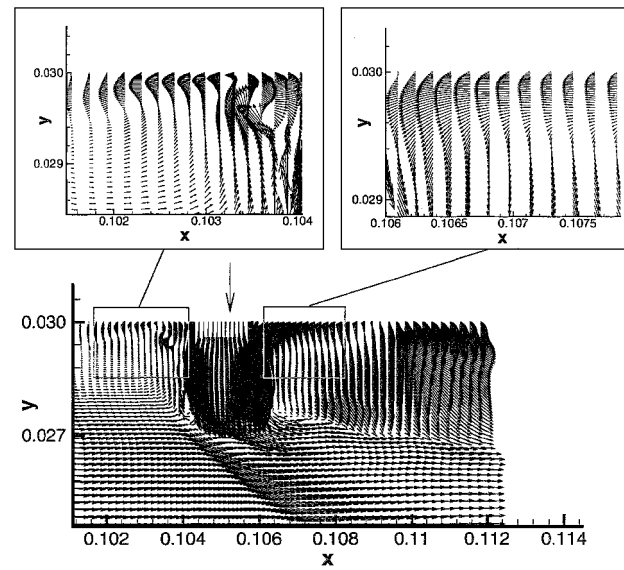

Fig. 5 Velocity vectors on the centerline.

be recognized by the nonzero water concentration upstream of the jet. In agreement with the experimental measurements published in Ref. 31, the H_2O is carried upstream of the injection opening by recirculating fluid in the boundary layer. Downstream of the region immediately at the H_2 jet where most of the H_2O production occurs, the flow is basically chemically frozen, with H_2O being convected. Some of the H_2 reacts with the surrounding air in the free shear layer. The ondulation of the H_2O contours is a clear indication of the unsteady character of the flow.

To evaluate the present results statistically and to obtain an indication of the vorticity induced in the flow, the enstrophy, defined as $\frac{1}{2}(\nabla \times \boldsymbol{u}')^2$, was computed. The mean values of the velocity components were obtained by averaging the results of the last 300 μs. The result is given in Fig. 8. The H_2 jet appears prolongated due to a grid stretching in the direction perpendicular to the main flow. The top part of Fig. 8 shows a side view of the jet and a region behind it; the bottom part shows a top view of the same flowfield. One can recognize three areas of high enstrophy. First, the sides of the jet are associated with high enstrophy due to the fluctuating motion of the same. Second, behind the jet, there is an area of high

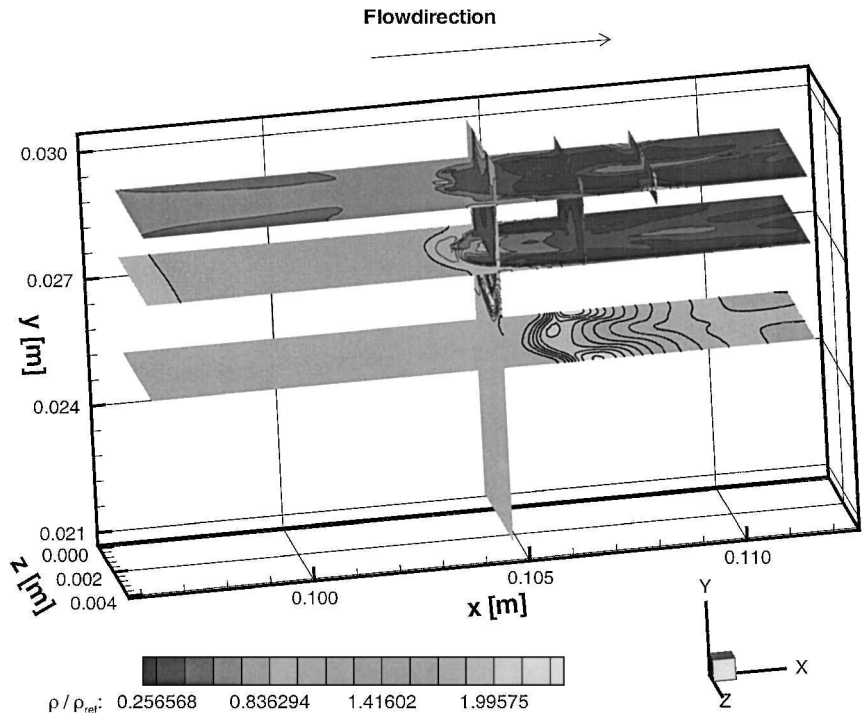

Fig. 6 Density contours at the injection hole.

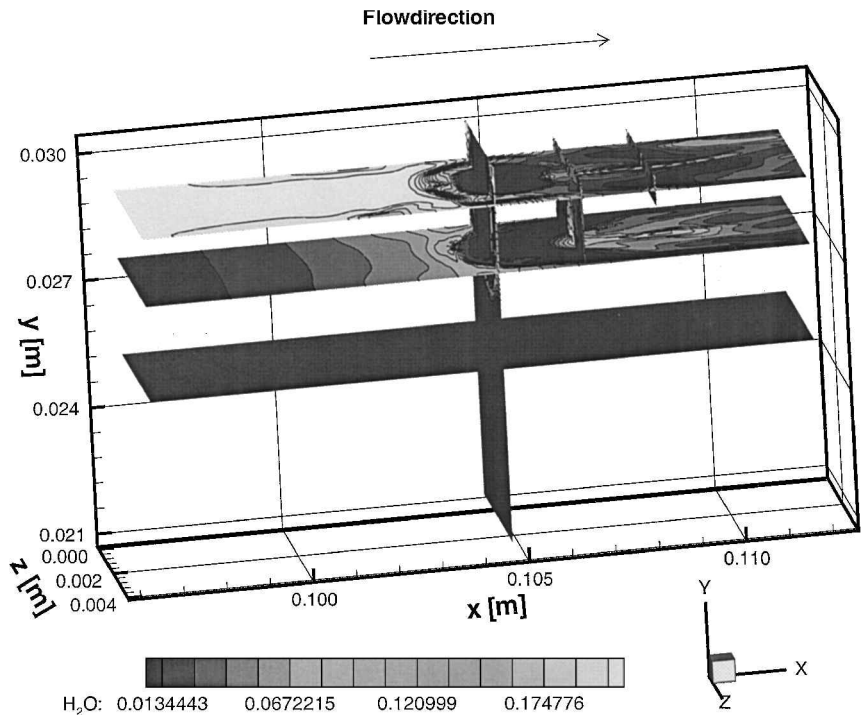

Fig. 7 Water concentration at the injection hole.

turbulence, enhancing the mixing of H_2 and air and, therefore, also the rate of combustion. Third, the boundary layer at the top wall, especially under the horseshoe vortex, is highly vortical, reflecting an increased level of turbulence. This region is very thin and barely visible in the side view, but is dominant in the top view.

The turbulent kinetic energy spectrum is shown in Fig. 9 at a location 5 mm behind the H_2 jet in the outer part of the boundary layer, 1 mm off the centerline. Although part of the eddies with the largest energy contents have been captured, only two orders of magnitude are covered by the LES, whereas at least three would be more desirable. On the other hand, it can be argued that most of the combustion will take place outside of the boundary layer, mainly in the unsteady region at and behind the H_2 jet and in the free shear layer downstream of it, where most of the larger eddies have been resolved.

The measured[31] and computed velocities at the end of the channel considered in the present simulation are compared in Fig. 10. The three-dimensional simulation results in velocities that are in fair agreement with the experimental data, although the measured velocities were obtained by averaging over approximately 400 μs,

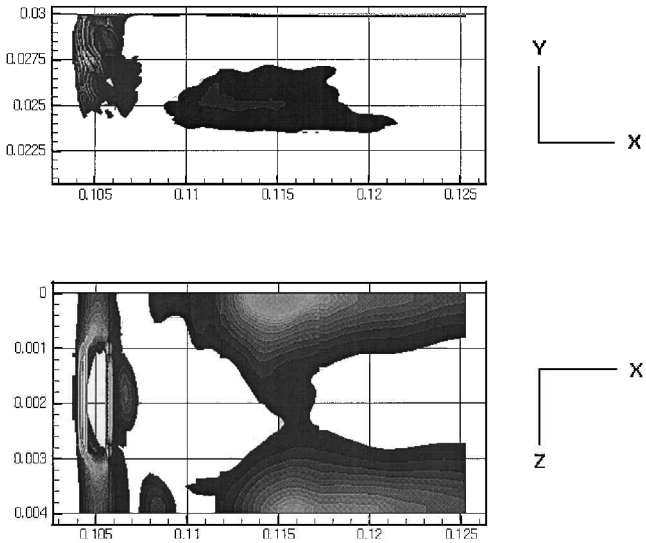

Fig. 8 Isosurface of the grid scale enstrophy at and behind the hydrogen jet.

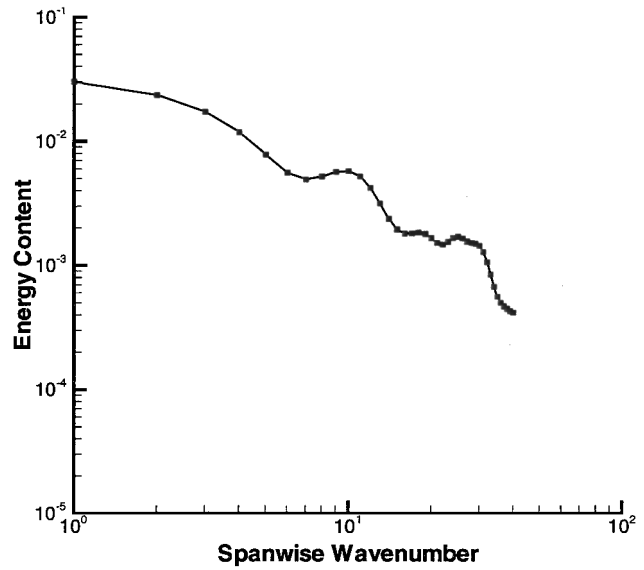

Fig. 9 Turbulent kinetic energy spectrum.

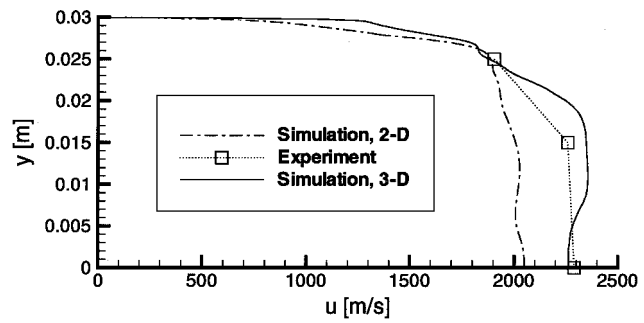

Fig. 10 Comparison of computed (present) and measured[26] time-averaged velocities at the end of the simulated channel.

whereas the numerically determined velocities were averaged only over 90 μs. The two-dimensional results, on the other hand, agree with the experiment rather poorly.

Finally, the simulated schlieren picture of the flow at and downstream of the injection position is compared with its experimental counterpart in Fig. 11. Although shown at a different vertical scale, the similarity can be clearly recognized. In particular, the location and shape of the oblique shocks and the extent of the turbulent shear

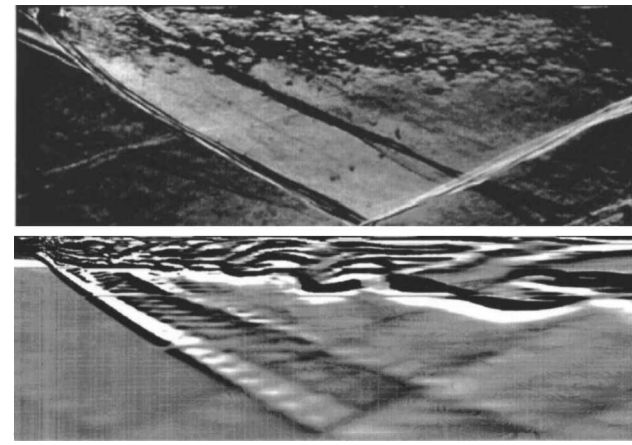

Fig. 11 Comparison of the numerical (lower) and experimental (upper) schlieren pictures of the reacting flow at and downstream of H_2 injection.

layer agree rather well. The structure of the numerically generated shear layer is similar to the experimental picture at the injection, where the resolution is sufficiently high, but becomes coarser downstream as the gird resolution rapidly decreases.

VIII. Conclusions

The main goal of the present work was the numerical simulation of a small yet important component of a simple supersonic combustion chamber. Here, the flowfield in a part of a supersonic channel with transverse hydrogen injection, containing one injection opening, was predicted using the present solver of compressible viscous chemically reacting flows. This configuration is the subject of experimental studies being undertaken by many academic and research institutions and is, therefore, of significant importance. The resulting flowfield was highly unsteady, with periodic motion of the H_2 jet and the free shear layer downstream of the location of the injection port. Although no quantitative comparison with corresponding steady-state computations has been made, it can be argued that the unsteady combustion process must be different due to enhanced mixing. The difference between the two-dimensional and three-dimensional results was to be expected, but it was larger than anticipated, making two-dimensional simulations of this class of flow questionable. Most of the experimentally observed flow features, such as barrel shock, bow shock, horseshoe vortex, and separation regions upstream and downstream of the injection port could be recognized in the present numerical results.

The present LES was able to capture some of the large-scale turbulent effects in the boundary layer downstream of the H_2 jet and in the free shear layer, at a significant computational cost. Even so, the resolution should be further increased in future work to capture more of the turbulent kinetic energy spectrum. The effect of turbulence on the nonequilibrium chemistry was accounted for only by considering the temperature fluctuations. In the present special case, this might be an acceptable simplification, but generally, but generally the PDF transport equations for mass fractions must be considered as well.

Future work must concentrate on improving the chemical reaction model, which is much too simple. The computer program must be made more efficient by, for example, precomputing the chemical source terms only once into a matrix and interpolating the proper values during the iterative solution process. The addition of a better subgrid model or the implementation of the FDF equations are necessary and will be carried out in the near future.

Acknowledgments

The present work was supported by a grant from the German Research Association. The major part of the computer resources were provided by a grant from the High Performance Computer Center for Science and Research at the Research Center Jülich GmbH, Germany.

References

[1]Rausch, V. L., McClinton, C. R., and Hicks, J. W., "Scramjets Breathe New Life into Hypersonics," *Aerospace America*, No. 7, July 1997, pp. 40–46.

[2]Covault, C., "Hypersonic Strategy Sets Stage for 'Next Great Leap," *Aviation Week and Space Technology*, No. 11, March 2001, pp. 28–30.

[3]Brummund, U., and Nuding, J.-R., "Interaction of Compressible Shear Layer with Shock Waves: an Experimental Study," AIAA Paper 97-0392, 1997.

[4]Cox, C. F., Cinnella, P., and Arabshahi, A., "Multi-Block Calculations for Flows in Local Chemical Equilibrium," AIAA Paper 93-2999, July 1993.

[5]Godfroy, F., and Tissier, P. Y., "CFD Analysis of Vortex Shedding Inside a Subscale Segmented Motor," AIAA Paper 94-2781, June 1994.

[6]Madabhushi, R. K., Choi, D., Barber, T. J., and Orszag, S., "Computational Modeling of Mixing Process for Scramjet Combustor Applications," AIAA Paper 97-2638, July 1997.

[7]Chen, K.-H., and Shuen, J.-S., "A Comprehensive Study of Numerical Algorithms for Three-Dimensional, Turbulent, Nonequilibrium Viscous Flows with Detailed Chemistry," AIAA Paper 95-0800, 1995.

[8]Chamberlain, R., Dang, A., and McClure, D., "Effect of Exhaust Chemistry on Reaction Jet Control," AIAA Paper 99-0806, 1999.

[9]von Lavante, E., Hilgenstock, M., and Groenner, J., "Simple Numerical Method for Simulating Supersonic Combustion," AIAA Paper 94-3179, June 1994.

[10]Hilgenstock, M., von Lavante, E., and Groenner, J., "Efficient Computations of Navier–Stokes Equations with Nonequilibrium Chemistry," American Society of Techanical Engineers, ASME Paper 94-GT-251, 1994.

[11]Narayan, J. R., "Prediction of Turbulent Reacting Flows Related to Hypersonic Airbreathing Propulsion Systems," AIAA Paper 94-2948, June 1994.

[12]Möbius, H., Gerlinger, P., and Brüggemann, D., "Monte Carlo PDF Simulation of Compressible Turbulent Diffusion Flames Using Detailed Chemical Kinetics," AIAA Paper 99-0198, 1999.

[13]Chakravarthy, V. K., and Menon, S., "Characteristics of a Subgrid Model for Turbulent Premixed Combustion," AIAA Paper 97-3331, July 1997.

[14]Menon, S., "Subgrid Combustion Modelling for Large-Eddy Simulation," *International Journal of Engine Research*, Vol. 1, No. 2, 2000, pp. 209–227.

[15]Arunajatesan, S., and Menon, S., "Simulation of Controlled Injection of Toxic Waste for Enhanced Destruction in a Compact Incinerator," AIAA Paper 96-3075, July 1996.

[16]Colucci, P. J., Jaberi, F. A., Givi, P., and Pope, S. B., "Filtered Density Function for Large Eddy Simulations of Turbulent Reactive Flows," *Physics of Fluids*, Vol. 10, No. 2, 1998, pp. 499–515.

[17]Kallenberg, M., and von Lavante, E., "The Dynamics of Unsteady Supersonic Combustion," AIAA Paper 98-3319, July 1998.

[18]Evans, J. S., Schexnayder, C. J., "Influence of Chemical Kinetics and Unmixedness on Burning in Supersonic Hydrogen Flames," *AIAA Journal*, Vol. 18, No. 2, 1980, pp. 188–193.

[19]Roe, P. L., and Pike, J., "Efficient Construction and Utilisation of Approximate Riemann Solutions," *Computing Methods in Applied Sciences and Engineering VI, Proceedings of Sixth International Symposium on Computing Methods in Applied Sciences and Engineering*, North-Holland, 1984, pp. 499–516.

[20]van Leer, B., "Flux-Vector-Splitting for the Euler Equations," Inst. for Computer Applications in Science and Engineering, Hampton, VA, Rept. 82-30, Sept. 1982.

[21]Liou, M. S., "On a New Class of Flux Splitting," *Proceedings of the 13th International Conference on Numerical Methods in Fluid Dynamics*, 1992, pp. 115–119.

[22]Grossmann, B., and Cinella, P., "Flux-Split Algorithms for Flows with Non-Equilibrium Chemistry and Vibrational Relaxation," *Journal of Computational Physics*, Vol. 88, No. 1, 1990, pp. 131–168.

[23]Larrouturou, B., and Fezoui, L., "On the Equations of Multi-Component Perfect or Real Gas Inviscid Flow," *Nonlinear Hyperbolic Problems*, Lecture Notes in Mathematics, Vol. 1402, *Proceedings of an Advanced Research Workshop*, Springer-Verlag, Heidelberg, Germany, 1989.

[24]Smagorinsky, J., "General Circulation Experiments with the Primitive Equations," *Monthly Weather Review*, Vol. 91, No. 3, 1963, pp. 401–419.

[25]Sattelmayer, T., "Selbstzündung, Flammenstabilisierung and Stoß-Flammen-Wechselwirkung in stoß-induzierten Überschallflammen," Bericht des Sonderforschungs-bereichs 255 der TU-München, Munich, June 2001.

[26]von Lavante, E., "The Accuracy of Upwind Schemes Applied to the Navier–Stokes Equations," *AIAA Journal*, Vol. 28, No. 7, 1990, pp. 975–984.

[27]Lugt, H. J., "Wirbelstroemung in der Natur und Technik," G. Braun Karlsruhe, Germany, 1979.

[28]Truckenbrodt, E., "Fluidmechanik," Springer-Verlag, 1989.

[29]Faden, M., "Interaktive Simulation Instationaerer Stroemungen auf einem massiven parallelen Rechner," Dissertation Universitaet Essen, Germany, 1993.

[30]Ramakrishnan, and Singh, "Scramjet Combustor Flowfields," *AIAA Journal*, Vol. 32, No. 5, 1994, pp. 930–935.

[31]Quenett, C., "Stoßrohruntersuchungen zur H_2—Verbrennung in einer heissen Überschallströmung," Ph.D. Dissertation Univ. of Essen, Essen, Germany, 1995.